

# 13 Years of Timing of PSR B1259–63

N. Wang<sup>1,2,3</sup>, S. Johnston<sup>1</sup> & R. N. Manchester<sup>2</sup>

<sup>1</sup> School of Physics, University of Sydney, NSW 2006, Australia

<sup>2</sup> Australia Telescope National Facility, CSIRO, P.O. Box 76, Epping NSW 1710, Australia

<sup>3</sup> Urumqi Astronomical Observatory, NAOC-CAS, 40-5 South Beijing Road, Urumqi, China, 830011

20 March 2018

## ABSTRACT

This paper summarizes the results of 13 years of timing observations of a unique binary pulsar, PSR B1259–63, which has a massive B2e star companion. The data span encompasses four complete orbits and includes the periastron passages in 1990, 1994, 1997 and 2000. Changes in dispersion measure occurring around the 1994, 1997 and 2000 periastrons are measured and accounted for in the timing analysis. There is good evidence for a small glitch in the pulsar period in 1997 August, not long after the 1997 periastron, and a significant frequency second derivative indicating timing noise. We find that spin-orbit coupling with secular changes in periastron longitude and projected semi-major axis ( $x$ ) cannot account for the observed period variations over the whole data set. While fitting the data fairly well, changes in pulsar period parameters at each periastron seem ruled out both by X-ray observations and by the large apparent changes in pulsar frequency derivative. Essentially all of the systematic period variations are accounted for by a model consisting of the 1997 August glitch and step changes in  $x$  at each periastron. These changes must be due to changes in the orbit inclination, but we can find no plausible mechanism to account for them. It is possible that timing noise may mask the actual changes in orbital parameters at each periastron, but the good fit to the data of the  $x$  step-change model suggests that short-term timing noise is not significant.

**Key words:** Binaries: general – pulsars: individual: PSR B1259–63

## 1 INTRODUCTION

PSR B1259–63 was discovered in a large-scale high frequency survey of the Galactic plane (Johnston et al. 1992a). It is unique because it is the only known radio pulsar in orbit about a massive, main-sequence, B2e star (Johnston et al. 1992b). PSR B1259–63 has a short spin period of  $\sim 48$  ms and moderate period derivative of  $2.28 \times 10^{-15}$ , implying a characteristic age of only 330 kyr from spin-down by magnetic dipole radiation. It has an orbital period of  $\sim 1237$  days, and an eccentricity of 0.87, the longest orbital period and largest eccentricity of any of the known binary radio pulsars. The inclination of the orbit to the plane of the sky is  $i \sim 36^\circ$ .

The companion, SS 2883, is a 10th magnitude star with a mass of about  $10 M_\odot$  and a radius of  $6 R_\odot$ . Typical of Be stars as a class, it has a hot, tenuous polar wind and a cooler, high density, equatorial disk. The mass loss rate of the B2e star is  $\sim 10^{-6} M_\odot$ . Johnston et al. (1994) observed H $\alpha$  emission lines from the disk at 20 stellar radii ( $R_*$ ), just inside the pulsar orbit of  $24 R_*$  at periastron. The density of the disk material is high near the stellar surface ( $10^8 -$

$10^{10} \text{ cm}^{-3}$ ), and falls off as a power-law with distance from the star. The disk is likely to be highly tilted with respect to the pulsar orbital plane, and PSR B1259–63 is eclipsed for about 40 days as it goes behind the disk.

Assuming the B2e star is rotating at  $\sim 70$  per cent of its break up velocity (Porter 2001), SS 2883 then has an equatorial velocity  $\sim 280 \text{ kms}^{-1}$ . The spin-induced oblateness of the star implies an additional  $1/r^3$  gravitational potential term in the interaction with the pulsar, known as quadrupole gravitational moment in typical binary system. This effect introduces an apsidal motion and precession of the orbital plane if the spin of the companion is not aligned with the orbit angular momentum, characterised by  $\dot{\omega}$  and  $\dot{i}$  respectively, where  $\omega$  is the longitude of periastron passage and  $x$  is the projected pulsar semi-major axis (Lai, Bildsten & Kaspi 1995).

In an eccentric binary system, the passage of the pulsar through periastron excites tidal motions on the companion star which then interact with the orbital motion. In the case of PSR J0045–7319 (Kaspi et al. 1996), tidal effects may account for the observed evolution in binary parameters (e.g. Lai 1997). The tidal interactions may be enhanced by large

factors if there is a resonance with oscillation modes of the star (Witte & Savonije 1999). For PSR J0045–7319, at periastron the pulsar is only  $\sim 4 R_*$  from the companion compared to  $24 R_*$  for PSR B1259–63. Tidal effects are strongly dependent on the separation of the two stars, and so may be insignificant in PSR B1259–63.

Interactions between the pulsar and the disk of the Be star may also be important. If there is accretion from the disk on to the neutron star, the pulsar may be spun up or slowed down. For accretion to occur, the bow shock, where there is pressure balance between the pulsar wind and the Be-star disk gas, must lie inside the accretion radius, which depends on relative velocity of the pulsar and the accreting gas. For PSR B1259–63, accretion is unlikely (Manchester et al. 1995; Kaspi et al. 1995; Tavani & Arons 1997), with X-ray observations (Hirayama et al. 1999) most easily interpreted as originating from a bow shock well outside the pulsar magnetosphere. Disk interactions may also affect pulsar orbit directly through frictional drag. Estimates (Manchester et al. 1995; Wex et al. 1998) of variations in the Keplerian parameters  $P_b$ ,  $\omega$  and  $e$  suggest the effect is negligible.

Timing models for binary pulsars have evolved over the years, mainly to take into account general relativistic effects (Blandford & Teukolsky 1976; Damour & Deruelle 1986). Wex (1998) extended these models to deal with long-period systems with main sequence companions. His model, the so-called MSS model, accounts for short-term periodic orbital effects and for the long-term secular effects caused by classical spin-orbit coupling.

The latest paper on timing of PSR B1259–63 (Wex et al. 1998) analysed observations from 1990 January to 1996 December which covered the 1990 and 1994 periastron passages. Wex et al. (1998) were unable to derive a unique timing model for the system, partly because of the large timing noise and partly due to the long eclipses of the pulsed emission. They put forward two possible solutions for the timing. In one, timing noise dominated, its effects were removed through higher order derivatives of the spin frequency, and there was no orbital precession or tidal effects. In the second model, which they preferred, significant values of  $\dot{\omega}$  and  $\dot{x}$  were obtained. These were interpreted as being due to orbital precession, and a large tilt between the rotation axis of the Be star and the orbital angular momentum vector was inferred. Two different fits were obtained for  $\dot{\omega}$  and  $\dot{x}$  depending on the number of (integer) rotations added during the 1994 eclipse. The preferred solution then relied on the physical interpretation of the values of  $\dot{\omega}$  and  $\dot{x}$ .

Since then, we have obtained a further six years of timing data on this pulsar to give a total data span of 13 years, including two further periastron passages in 1997 and 2000. Our main findings are: (1) that there is strong evidence for a pulsar period glitch in 1997 August, about 94 days after the 1997 periastron, (2) that the Wex et al. (1998) timing solution which included orbital precession does not remain valid through the 1997 and 2000 periastrons, (3) that a solution with jumps in  $\nu$  and  $\dot{\nu}$  at each periastron, while fitting the data reasonably well, is unlikely to be physically viable, and (4) that the data are best explained by a combination of the 1997 August pulsar glitch and steps in projected orbit semi-major axis ( $x$ ) at each periastron. However, the possible presence of timing noise and the long-duration eclipses

conspire to make timing of the pulsar difficult. In Section 2 we discuss details of the observations and data analysis techniques, Section 3 describes the pulse profile evolution from 0.66 to 13.6 GHz and Section 4 describes the dispersion measure variations observed around the 1994, 1997 and 2000 periastrons. The timing results are described in Section 5 with fits of the various possible models, and the possible interpretations are discussed in Section 6.

## 2 OBSERVATIONS AND ANALYSIS

We report here on observations of PSR B1259–63 using the Parkes radio telescope over a time interval of nearly 5000 days between 1990 January and 2003 June (MJD 47909 to 52804). A total of 1031 times of arrival (TOAs), spanning four orbital periods, were obtained for the pulsar. The majority of the observations were made at frequencies around 1.4 GHz with additional observations at 0.66, 2.4, 4.8, 8.4 and 13.6 GHz.

At 1.4 GHz, the H-OH receiver (Thomas, Greene & James 1990) with a system equivalent flux density of  $\sim 40$  Jy was used prior to 1997. From 1997, the multibeam receiver (Staveley-Smith et al. 1996), with a system equivalent flux density of  $\sim 28$  Jy, was employed. Short observations with duration  $\sim 10$  min were made at typically two-week intervals far from periastron. Longer observations with duration  $\sim 1$  hr were made on a daily basis at times close to periastron. The higher frequency observations were generally conducted close to the epochs of periastron in order to measure the dispersion measure changes and the scatter broadening of the pulse profile (Johnston et al. 2001). The receivers at 4.8 and 8.4 GHz had system equivalent flux densities of  $\sim 100$  Jy. Lower frequency observations were more rarely performed. The combination of increased Galactic background emission at low frequencies, and the flat spectral index of the pulsar, made it hard to detect.

The backend systems included various combinations of filterbanks and correlators. Table 1 lists the details of the observing systems. Filterbank systems were used throughout the observation period. At frequencies above 1 GHz, they generally consisted of 64 frequency channels each of width 5 MHz (1991–1997), 96 channels of width 3 MHz (1997–2003) or 512 channels of width 0.5 MHz (2001 onwards). The filterbank backends were only capable of measuring total power. They one-bit sampled the data typically at intervals of  $600 \mu\text{s}$  for this pulsar. The data stream was written to tape for subsequent off-line analysis. This analysis involved de-dispersing and folding the data at the topocentric period. A digital correlator, the Caltech Fast Pulsar Timing Machine (FPTM; Navarro 1994), was in use between 1994 and 2001. It had 128 MHz of bandwidth with 128 frequency channels. When operating in total power mode, two independent 128 MHz bands were available. When full Stokes parameters were recorded, however, only one band could be used. The correlator performed on-line pulse-folding and dedispersion to produce a pulse profile with up to 1024 time bins per period. Further information for earlier observations can also be found in Wex et al. (1998) and Johnston et al. (2001).

The pulse profile of PSR B1259–63 consists of two, almost equal-strength components. Each component has a

**Table 1.** Detail of the observing systems used for PSR B1259–63. FB denotes a filterbank system and FPTM denotes the Caltech Fast Pulsar Timing Machine.

Freq (GHz)	Backend	Year	BW (MHz)	No. of Channels	No. of TOAs
0.66	FB	1990–1996	32	128	14
	FPTM	1995–1997	32	128	13
1.4	FB	1990–1997	320	64	243
	FB	1997–2003	288	96	101
	FB	2001	256	512	3
	FPTM	1994–2001	128	128	444
2.4	FPTM	1997–1998	64	128	4
	FB	1992–1993	320	64	11
4.8	FPTM	2000–2001	128	128	4
	FB	1993–1997	320	64	33
	FB	1997	576	192	24
8.4	FPTM	1996–2001	128	128	78
	FB	1993–1996	320	64	21
	FB	1997	576	192	5
13.6	FPTM	1996–1997	128	128	17
	FPTM	1995	128	128	15

**Table 2.** Details of the observation data spans.  $\tau+$  is the first detection of the pulsar after the preceding periastron and  $\tau-$  is the final detection prior to the following periastron.

Data span	Preceding Periastron (MJD)	$\tau+$ (d)	$\tau-$ (d)	No. of TOAs
1990.1–1990.7	–	–	107	18
1990.7–1994.0	48124	171	20	187
1994.0–1997.5	49361	24	18	443
1997.5–2000.9	50597	16	52	237
2000.9–2003.5	51834	19	–	146

step edge and a more slowly falling edge. Manchester & Johnston (1995) suggested that the steep edges were the outside of a cone with large opening angle. In order to obtain a good value for the dispersion measure, it is important that the profile be properly aligned over the entire frequency range between 0.66 and 13.6 GHz. We chose the point midway between the mid-points of the steep outer edges as the fiducial point. At each frequency, a large number of profiles were summed together to form a high signal-to-noise template. These templates are shown in Fig.1. To obtain an accurate TOA we then cross-correlated individual observations with the relevant template.

Table 2 lists the epoch of periastron for each of the four orbits so far observed. It lists the total number of TOAs obtained during the orbit, and indicates the first detection of the pulsar after periastron and the final detection of the pulsar before it enters the eclipse.

The eclipses of the pulsar, which last for  $\sim 40$  days around periastron make the timing difficult. The problem is exacerbated by the fact that DM changes are observed over a few tens of days leading up to and immediately following the eclipse due to the changing line of sight intersecting the Be star wind. These DM variations need to be removed to obtain a good timing solution, and this involves making observations at several different frequencies as near

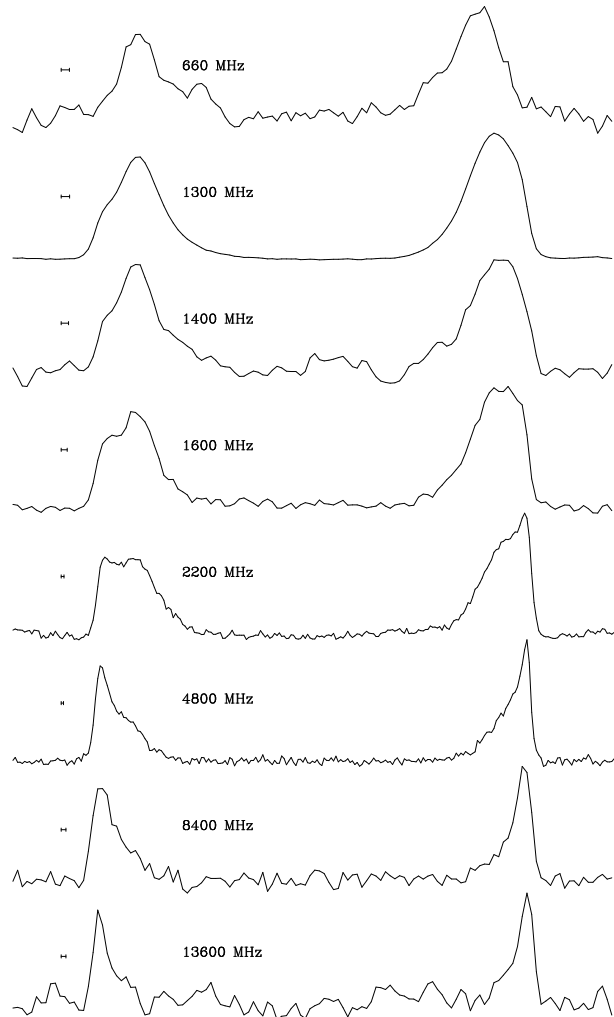


**Figure 1.** Standard profiles of PSR B1259–63, summed from individual observations. The bar on the left side of the profiles is the effective resolution, including the effects of DM smearing.

to simultaneously as possible. Multi-frequency observations were therefore made before and after the 1994, 1997 and 2000 periastron passages and have been described in detail in Johnston et al. (1996) and Johnston et al. (2001). Generally, observations were made at 5 different frequencies, 1.2, 1.4, 1.5, 4.8 and 8.4 GHz. The three frequencies near 1.4 GHz were obtained simultaneously and the observation would then be followed by one at either 4.8 or 8.4 GHz before again observing at the lower frequencies.

In order to measure an accurate DM we assume that the DM contribution from the 1.5 kpc along the line of sight through the interstellar medium is  $146.8 \text{ pc cm}^{-3}$  (Connors et al. 2002). Then the extra DM contribution from the disk of the Be star could be computed from the relative difference in the timing residuals between the different frequencies. Typical errors using this method are  $\sim 0.1 \text{ pc cm}^{-3}$ .

The timing properties were analysed using the pulsar timing program TEMPO<sup>\*</sup>, which provides least-squares fitting to the pulsar rotation and orbital parameters and the

\* See <http://www.atnf.csiro.au/research/pulsar/timing/tempo/>

dispersion measure. The MSS binary model of Wex (1998) was used for all fits except those in Section 5.6. To fit for steps in the orbital parameters, a new binary model (BTJ) based on the BT model (Blandford & Teukolsky 1976) was implemented. This allows cumulative steps in longitude of periastron ( $\omega$ ), projected semi-major axis ( $x$ ), eccentricity ( $e$ ) and binary period ( $P_b$ ) to be inserted at specified times and also allowed setting or solving for jumps in pulsar phase at the specified times.

We note that our results differ slightly from those of Wex et al. (1998) when analysing the same data set. This is because new standard profile templates were used and the dispersion analysis re-done for this work.

### 3 PULSE PROFILE EVOLUTION

Fig. 1 shows that the pulse profile evolves substantially over the observed range from 660 to 13600 MHz. At first glance it appears that the profile gets narrower (when plotted as in Fig. 1) at lower frequencies, the opposite trend to that observed in most conal profiles. However, a closer examination suggests that this apparent width variation is largely due to differing spectral index of components making up each peak of the profile. The outer components are stronger at higher frequencies whereas components on the inner edge of each peak become strong at lower frequencies and dominate the profile at frequencies below 2 GHz. The flatter spectral index for outer conal components is commonly observed in other conal pulsars (Rankin 1983; Lyne & Manchester 1988) and reinforces the interpretation that the steep edges define the boundary of a wide emission cone from a single polar region (cf. Manchester 1996).

### 4 DM VARIATIONS

As PSR B1259–63 approaches periastron and moves into the Be-star disk, electron density variations along the line of sight result in DM changes as a function of orbital phase. Fig. 2a shows the observed variations from 1992, covering the 1994, 1997 and 2000 periastrons, and Fig. 2b shows expanded plots for  $\pm 75$  days about the periastrons. DM variations for the 1994 periastron were reported by Johnston et al. (1996), and for the 1997 periastron these were monitored extensively and reported by Johnston et al. (2001), while the 2000 variations have not been previously reported.

At the 1994 periastron, a peak of  $10.7 \pm 0.2 \text{ pc cm}^{-3}$  for  $\Delta\text{DM}$  was observed at  $\tau - 30$ ; after this it decreased with some fluctuations until the pulsar was eclipsed. In 1997, the peak was  $7.7 \text{ pc cm}^{-3}$  at  $\sim \tau - 28$ , slightly later than in 1994, and again the  $\Delta\text{DM}$  drops with some fluctuations until the pulsar is eclipsed at  $\sim \tau - 18$ . There are no multi-frequency data prior to the 2000 periastron. The points of  $\Delta\text{DM}$  in Fig. 2 are derived by extrapolating a timing solution based on observations in the 60 days before these pre-periastron points shown in Fig. 2b. The latest pre-periastron point is 52 days before the periastron. Based on the 1994 and 1997 behaviour, the peak of  $\Delta\text{DM}$  was not observed.

The  $\Delta\text{DM}$  fluctuations are well observed after the 1997 and 2000 periastrons. The  $\Delta\text{DM}$  values are much smaller

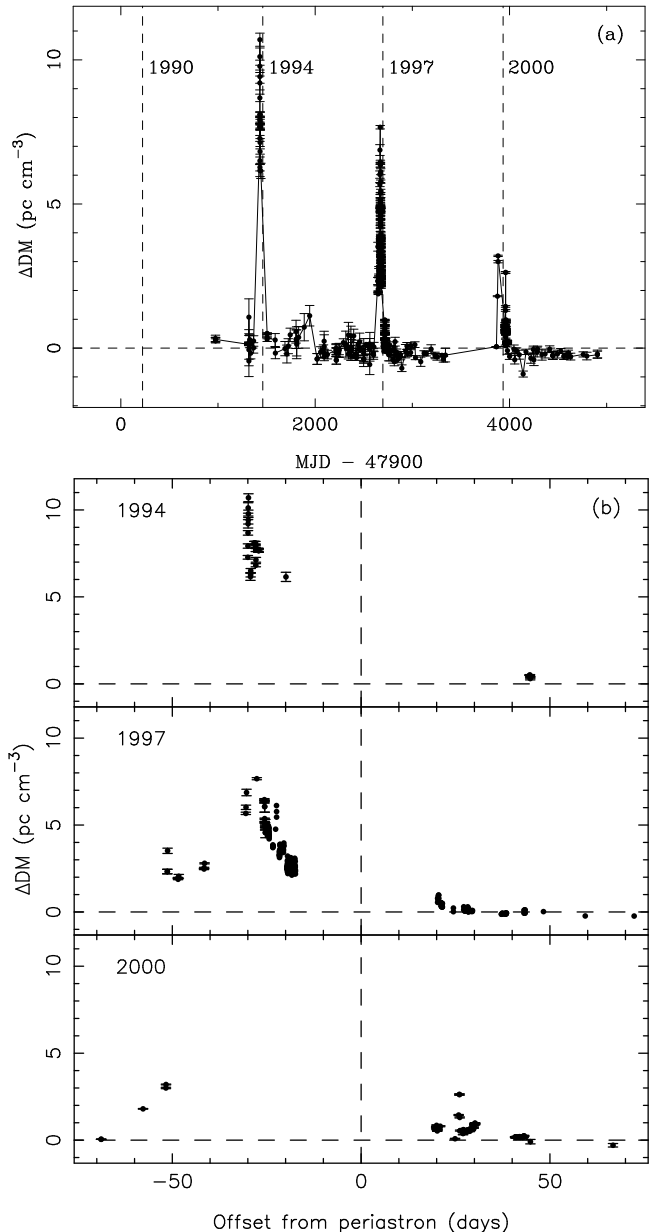


**Figure 2.** (a) Dispersion measure variations from 13 years of timing observation. The four vertical lines in this and subsequent plots represent 1990, 1994, 1997 and 2000 periastrons for PSR B1259–63. (b) Expanded plots for DM variations  $\pm 75$  days around periastron. The offset is measured relative to the value of  $146.8 \text{ pc cm}^{-3}$ .

than before periastron and approach zero about 30 days after periastron. In fact, Fig. 2 (a) shows that the  $\Delta\text{DM}$  values are slightly negative in mid-orbit, suggesting the reference DM value of  $146.8 \text{ pc cm}^{-3}$  is too large. The filterbank observations from  $\tau + 43$  after the 2000 periastron to the end of the data set gives a mean offset of  $-0.2 \pm 0.1 \text{ pc cm}^{-3}$  from the reference value; corresponding to an interstellar dispersion of  $146.6 \pm 0.1 \text{ pc cm}^{-3}$ .

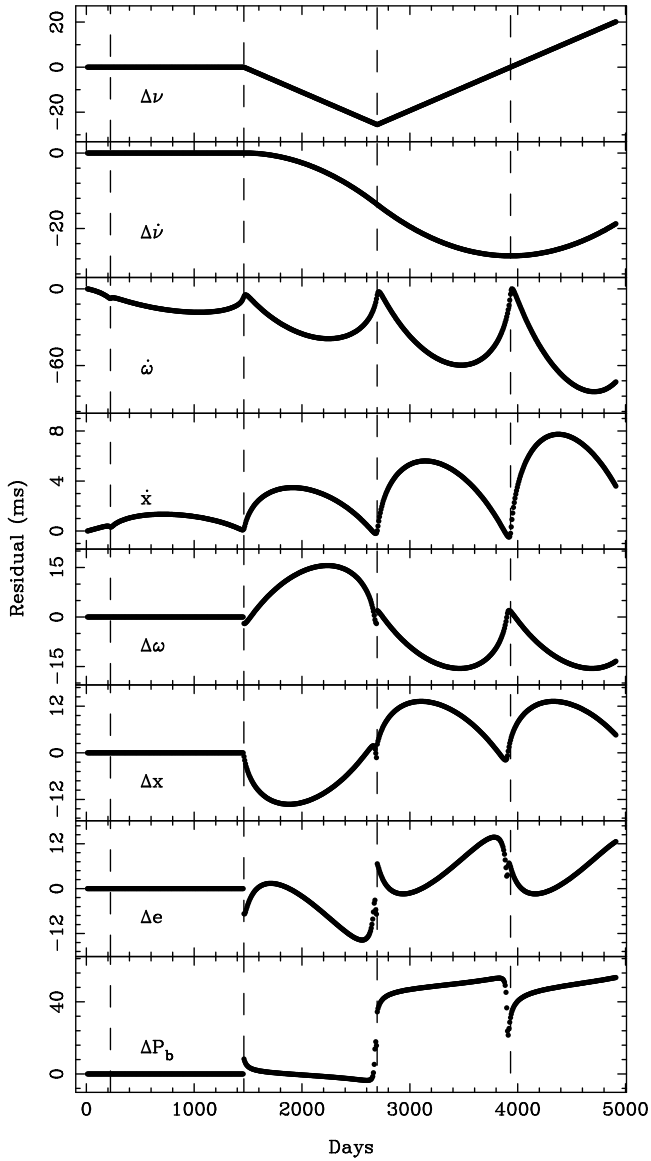


**Figure 3.** Simulated timing residuals after including jumps in  $\nu$  and  $\dot{\nu}$  (top two panels), constant  $\dot{\omega}$  and  $\dot{x}$  (next two panels) and jumps in orbital parameters (bottom four panels). Jumps were inserted at the second and third periastrons. See text for details.

## 5 TIMING RESULTS

### 5.1 Simulations

We first used simulations to determine the shape and amplitude of timing residuals corresponding to various parameters used in the fitting procedure. Fig. 3 shows us the timing signatures of the various parameters and the size of the resultant phase perturbations. In the figure we have attempted to ensure that the resultant residuals were of the order of tens of milliseconds, similar to the residuals seen in the real data. Apart from the  $\dot{\omega}$  and  $\dot{x}$  simulations, we introduced steps at the second and third periastron passages, with the change at the third periastron being twice the magnitude and of opposite sign to the change at the second periastron. Since the changes are cumulative, this has the effect of reversing the sign of the perturbation at the third peri-

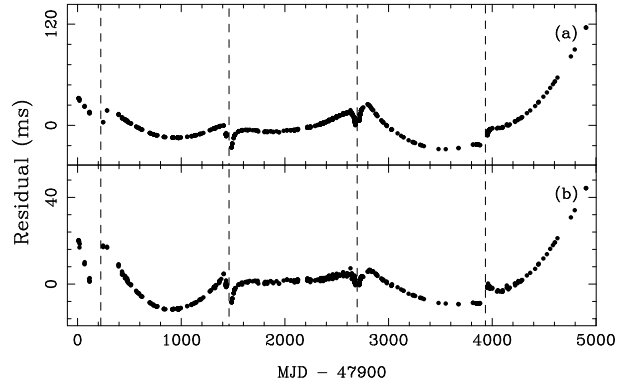


**Figure 4.** (a) Post-fit residuals after fitting for  $\nu$ ,  $\dot{\nu}$ ,  $\ddot{\nu}$  and the Keplerian orbital parameters. The rms residual is 14.6 ms. (b) Post-fit residuals with the 1997 August glitch (Section 5.6) included, giving an rms residual is 4.3 ms.

astron. The steps in  $\nu$  and  $\dot{\nu}$  at the second periastron are respectively  $5 \times 10^{-9} \text{ s}^{-1}$  and  $5 \times 10^{-17} \text{ s}^{-2}$ . For  $\dot{\omega}$  and  $\dot{x}$  we use the values from the Wex et al. (1998) model 2A of  $2 \times 10^{-4} \text{ deg yr}^{-1}$  and  $15 \times 10^{-12}$  respectively. The orbital parameter steps at the second periastron are  $\Delta\omega = 0^\circ.03$ ,  $\Delta x = 0.01 \text{ s}$ ,  $\Delta e = 4 \times 10^{-6}$  and  $\Delta P_b = 30 \text{ s}$  respectively.

### 5.2 A Glitch Near MJD 50691

After we had been through the process of fitting the data as described in the subsections below, it became apparent to us that there was strong evidence for a glitch in the pulsar period near MJD 50691 (1997 August 30), about 94 days after the 1997 periastron. The evidence for the glitch and its parameters are described more fully in Section 5.6 below. In each of the following subsections we describe the fits both with and without the glitch. In all cases except the final fit in Section 5.6, the glitch parameters are held fixed at the values determined in this final fit.

### 5.3 The Keplerian Timing Model

We initially attempted to fit the entire data set using the five Keplerian orbital parameters and the spin frequency and its first two time-derivatives. Wex et al. (1998) already showed that this did not fit the data well. The residuals for our extended data set are shown in Fig. 4a where the rms residual is 14.6 ms. The post-fit residuals after including the glitch shown in Fig. 4b are somewhat reduced with an rms residual of 4.3 ms, but still have large systematic variations. Parameters from this fit are given in the second column of Table 3. If we add four more higher-order spin frequency derivatives, the rms residual reduces to  $\sim 2.1 \text{ ms}$  but only at the expense of significantly more free parameters and still leaving systematic residuals. We note that in the timing residual plots (Fig. 4 – 7) residual error bars are not plotted since the TOA errors (typically  $< 100 \mu\text{s}$ ) are generally smaller than the plotted points. In general, systematic departures from the timing model dominate the residual plots.

**Table 3.** Four timing solutions for PSR B1259–63.

	No $\dot{\omega}$ , $\dot{x}$	$\dot{\omega}$ , $\dot{x}$	$\nu$ , $\dot{\nu}$ jumps	Orbital jumps
R.A. (J2000)	13 <sup>h</sup> 02 <sup>m</sup> 47 <sup>s</sup> .65(1)			
Dec. (J2000)	–63°50′08″.7(1)	–63°50′08″.7(1)	–63°50′08″.7(1)	–63°50′08″.7(1)
DM (pc cm <sup>–3</sup> )	146.8	146.8	146.8	146.8
$\nu$ (s <sup>–1</sup> )	20.93692453667(7)	20.9369245383(1)	20.93692435(4)	20.9369245339(9)
$\dot{\nu}$ ( $\times 10^{-12}$ s <sup>–2</sup> )	–0.9979077(6)	–0.9978663(7)	–0.9987(2)	–0.9979383(9)
$\ddot{\nu}$ ( $\times 10^{-24}$ s <sup>–3</sup> )	–2.11(2)	–1.96(2)	0.5(5)	–1.762(7)
Period epoch (MJD)	50357.00	50357.00	50357.00	50357.00
$x$ (s)	1296.315(2)	1296.282(2)	1296.3264(4)	1296.272(5)
$e$	0.8698869(5)	0.8698832(6)	0.8698902(2)	0.8698872(9)
$t_0$ (MJD)	48124.3491(1)	48124.3494(2)	48124.34892(3)	48124.34911(9)
$P_b$ (d)	1236.72404(3)	1236.72360(7)	1236.724259(7)	1236.72432(2)
$\omega$ (deg)	138.66588(7)	138.6644(1)	138.66624(6)	138.6659(1)
Glitch epoch (MJD)	50690.7	50690.7	50690.7	50690.7(7)
$\Delta\nu_g$ ( $\times 10^{-9}$ s <sup>–1</sup> )	67	67	67	67(1)
$\Delta\nu_d$ ( $\times 10^{-9}$ s <sup>–1</sup> )	22	22	22	22(1)
$\dot{\omega}$ (deg yr <sup>–1</sup> )	–	0.00020(1)	–	–
$\dot{x}$ ( $\times 10^{-12}$ )	–	127(5)	–	–
$\Delta\nu_{90}$ ( $\times 10^{-9}$ s <sup>–1</sup> )	–	–	0(3)	–
$\Delta\dot{\nu}_{90}$ ( $\times 10^{-15}$ s <sup>–2</sup> )	–	–	0.8(2)	–
$\Delta\nu_{94}$ ( $\times 10^{-9}$ s <sup>–1</sup> )	–	–	15(3)	–
$\Delta\dot{\nu}_{94}$ ( $\times 10^{-15}$ s <sup>–2</sup> )	–	–	0.19(5)	–
$\Delta\nu_{97}$ ( $\times 10^{-9}$ s <sup>–1</sup> )	–	–	–10(3)	–
$\Delta\dot{\nu}_{97}$ ( $\times 10^{-15}$ s <sup>–2</sup> )	–	–	–0.30(5)	–
$\Delta\nu_{00}$ ( $\times 10^{-9}$ s <sup>–1</sup> )	–	–	–2(3)	–
$\Delta\dot{\nu}_{00}$ ( $\times 10^{-15}$ s <sup>–2</sup> )	–	–	–0.33(5)	–
$\Delta x_{90}$ (ms)	–	–	–	60.3(7)
$\Delta x_{94}$ (ms)	–	–	–	–26.3(1)
$\Delta x_{97}$ (ms)	–	–	–	2.8(3)
$\Delta x_{00}$ (ms)	–	–	–	4.2(4)
No. TOAs	1031	1031	1031	1031
Rms residual (ms)	4.3	4.7	0.78	0.46

#### 5.4 Spin-orbit Coupling, $\dot{\omega}$ and $\dot{x}$

We next attempted to obtain a timing solution by adding in  $\dot{\omega}$  and  $\dot{x}$  to account for the spin-orbit coupling. As a starting point we used Model 2a from Wex et al. (1998) which used data up to the end of 1996. Fig. 5a shows this model extended to the entire data set. Clearly, its predictive power has failed and it does not track through the 1997 periastron. The residuals deviate immediately after the 1997 periastron and become worse again after the 2000 periastron. We then allowed the orbital parameters, the spin frequency and its first two derivatives and  $\dot{\omega}$  and  $\dot{x}$  to vary; the resultant fit is shown in Fig. 5b. The residual has an rms of 13.1 ms and shows significant deviations from white noise for the 1997 and 2000 orbits. The fitted values of  $\dot{\omega}$  and  $\dot{x}$  are 0.00029 deg yr<sup>–1</sup> and  $61 \times 10^{-12}$  respectively, both having changed sign from the Wex et al. (1998) solution. The post-fit residuals after including the glitch are shown in Fig. 5c. Again, this reduces the rms residual to 4.7 ms, but leaves systematic variations still unmodelled. Parameters from this fit are given in the third column of Table 3, showing that both  $\dot{\omega}$  and  $\dot{x}$  remain positive. Fitting for  $\dot{\omega}$  and  $\dot{x}$  changes the sign of  $\dot{x}$  and only reduces the rms residual to 4.0 ms.

#### 5.5 Jumps in $\nu$ and $\dot{\nu}$ at Periastrons

Our next attempt at a timing solution involved fitting for frequency and frequency derivative jumps at each of the

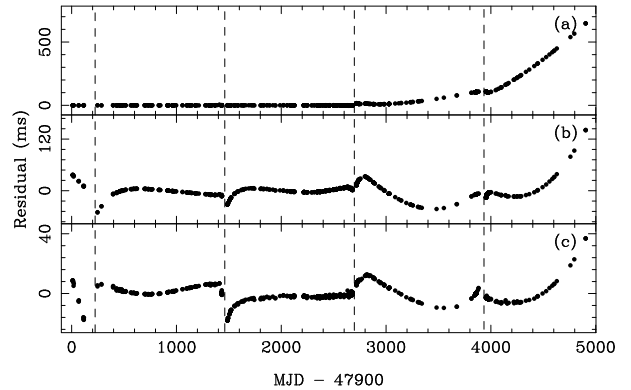


**Figure 5.** (a) Pre-fit timing residuals using the input parameters from model 2A of Wex et al. (1998). (b) Post-fit residuals after allowing all parameters to vary. We obtain  $\dot{\omega} = 0.00029(3)$  deg yr<sup>–1</sup> and  $\dot{x} = 61(14) \times 10^{-12}$ , and the rms residual is 13.1 ms. (c) Post-fit residuals with the 1997 August glitch included. The rms residual is 4.7 ms.

four periastron epochs (in a similar fashion to that done by Manchester et al. (1995) on a very early data set). Fig. 6a shows the residuals after fitting for the five orbital parameters, the rotation frequency and its first two derivatives and the jumps in  $\nu$  and  $\dot{\nu}$  at each periastron. The rms residual is now only 1.4 ms, and is a significant improvement on Fig. 4a and Fig. 5b, albeit at the expense of having 8 and

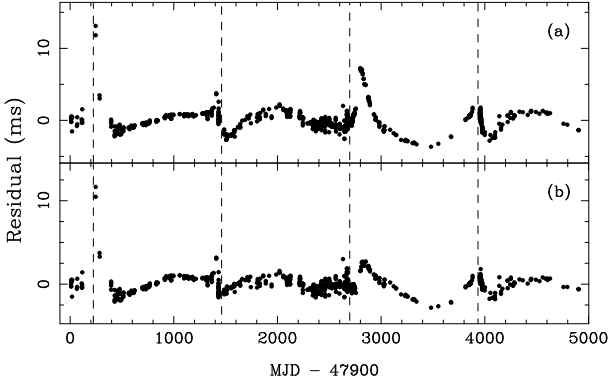


**Figure 6.** (a) Residuals after fitting for  $\nu$ ,  $\dot{\nu}$ ,  $\ddot{\nu}$ , the Keplerian orbital parameters and jumps in  $\nu$  and  $\dot{\nu}$  at each periastron, giving an rms residual of 1.4 ms. (b) Post-fit residuals after adding a glitch at MJD 50691. The rms residual is 0.78 ms.

6 extra free parameters respectively. Even this fit, however, does not remove the systematic deviations seen between the periastron passages.

The magnitude of the jumps in  $\nu$  are in the range  $10^{-9}$  to  $10^{-8} \text{ s}^{-1}$ . For the 1990 and 2000 periastrons they are negative, while for the 1994 and 1997 periastrons they are positive. All the jumps in  $\dot{\nu}$  are of negative sign, with amplitude  $\sim 10^{-16} \text{ s}^{-2}$ . However, after the glitch is included, several of the jumps in  $\nu$  and  $\dot{\nu}$  change sign:  $\Delta\dot{\nu}$  at the 1990 and 1994 periastrons become positive, while  $\Delta\nu$  at the 1997 periastron becomes negative. Parameters of this fit are shown in column four of Table 3 and the post-fit residuals are shown in Fig. 6b. The rms residual is now only 0.78 ms, and although some systematic variations are still seen, the fit is much better than for any previous fit. It should be noted that the jumps in  $\dot{\nu}$  have absorbed the overall  $\ddot{\nu}$  term (Table 3).

### 5.6 Jumps in Orbital Parameters at Periastron

From the results obtained so far, it seems clear that there are unmodelled effects still present in the data and that these effects vary from orbit to orbit but are not accounted for by secular changes in the orbital parameters. The next logical step is therefore to test the effect of jumps in the orbital parameters,  $\omega$ ,  $x$ ,  $e$  and  $P_b$ , at each periastron.

For the data set used by Wex et al. (1998), prior to the 1997 periastron, an excellent fit could be obtained by fitting for the pulsar frequency, its first two derivatives, the Kepler parameters and jumps in just  $x$  at the 1990 and 1994 periastrons. However, with the full data set and fitting for  $\Delta x$  at the remaining two periastrons, large systematic residuals were obtained. This fit is shown in Fig. 7a which has an rms residual of  $\sim 11$  ms. Even allowing for jumps in the other orbital parameters at any or all of the periastrons did not remove the systematic residual variations.

Examination of the post-fit residuals from many of the fits showed a sharp change of gradient near MJD 50691 (1997 August 30), about 94 days after the 1997 periastron, followed by a roughly exponential relaxation. This feature is most easily seen in Fig. 6a. Remarkably, fitting for this glitch in addition to jumps in just the projected semi-major axis at each periastron produced the almost featureless residuals

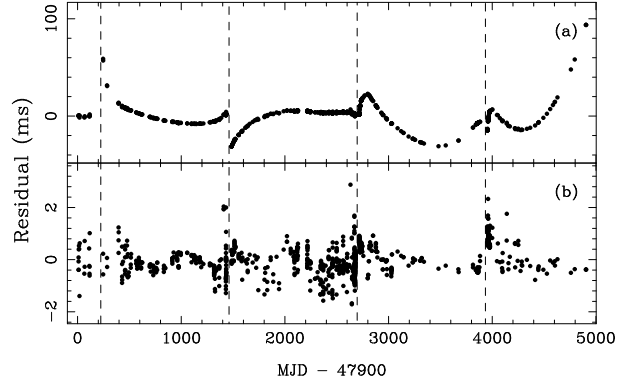


**Figure 7.** (a) Post-fit residuals for a fit of pulsar frequency and its first two derivatives, the Keplerian orbital parameters and jumps in the projected semi-major axis,  $x$ , at each periastron, giving an rms residual of 11 ms. (b) Post-fit residuals after the addition of a glitch at MJD 50691. The rms residual is now only 0.46 ms.

shown in Fig. 7b. The total frequency change at the time of the glitch, determined to be  $\text{MJD } 50690.7 \pm 0.7$ , was  $\Delta\nu_g = (67 \pm 1) \times 10^{-9} \text{ s}^{-1}$  of which  $\Delta\nu_d = (22 \pm 1) \times 10^{-9} \text{ s}^{-1}$  decayed exponentially with an assumed timescale of 100 days. The final rms residual is only 0.46 ms. Only a few points close to the periastrons are discrepant; these could easily be due to errors in the DM correction. Parameters for the fit shown in Fig. 7b are given in column five of Table 3.

## 6 DISCUSSION

### 6.1 Timing Noise

PSR B1259–63 is a relatively young pulsar with a large frequency derivative which is likely to have a high level of timing noise (Cordes & Downs 1985; Arzoumanian et al. 1994). Arzoumanian et al. (1994) proposed a measure of the timing noise to be

$$\Delta(t) = \log \left( \frac{|\ddot{\nu}|}{6\nu} t^3 \right) \quad (1)$$

where  $t$  is the time span over which the pulsar has been observed. For PSR B1259–63 we have  $t = 10^8$  s and for the measured value of the frequency and its second derivative we obtain  $\Delta_8 = -2.1$ . This is very close to the value for other pulsars with similar frequency derivatives, showing that PSR B1259–63 is typical in this respect.

The derived braking index,  $n = \nu\ddot{\nu}/\dot{\nu}^2$ , for PSR B1259–63 is  $-36.7$ . Again, this merely reflects the relatively high level of timing noise in this young pulsar (Johnston & Galloway 1999). The absence of systematic residual variations after fitting for steps in projected semi-major axis at each periastron (Fig. 7b) suggests that the timing noise is very red; higher-order derivatives in spin frequency are not significant.

### 6.2 Steps in Rotational Parameters

Fig. 6 shows that jumps in pulsar frequency and frequency derivative at periastron can account for most of the observed systematic residuals. As discussed by Manchester et

al. (1995), the most probable cause of frequency jumps at periastron is accretion of mass and angular momentum from the Be-star disk. The observed  $\Delta\nu$  are of order  $10^{-9}$  Hz, requiring accretion of about  $10^{20}$  g at the Alfvén radius of  $5 \times 10^7$  cm. While this amount of accreted mass is not unreasonable, there are several problems with this idea. Firstly, the bow shock between the pulsar wind and the circumstellar wind must lie inside the accretion radius for accretion to occur. Kaspi et al. (1995) and Tavani & Arons (1997) argued that this implies unreasonably high values for the disk density and/or outflow velocity. Secondly, the observed  $\Delta\nu$  are of different magnitudes and signs at the different periastrons. While there is evidence from the unpulsed continuum emission that wind parameters vary from one periastron to the next (Connors et al. 2002), it would be surprising if the accretion torque were able to change sign.

A further problem with this explanation for the observed timing residuals is that frequency jumps alone do not account for the observed variations; jumps in frequency derivative are also required. In fact, the  $\dot{\nu}$  jumps are generally more significant than the jumps in  $\nu$  (Table 3). The implied changes in braking torque or moment of inertia are large and physically improbable. These changes in  $\dot{\nu}$  could result from timing noise, but the fact that they are concentrated at the periastrons suggests that this is unlikely.

### 6.3 Changes in Orbital Parameters

It is clear from Section 5.4 that secular changes in  $\omega$  and  $x \equiv a \sin i$  do not account for the observed timing behaviour of PSR B1259–63, although it worked well for the first two periastrons. This is reinforced by the fact that the fitted jumps in  $x$  (Section 5.6) are of different sign at the different periastrons. This appears to mean that the conclusions drawn by Wex et al. (1998) about the inclination of the Be-star spin axis to the orbital plane may no longer be valid. We note that the  $\dot{x}$  measured by Wex et al. (1998) is roughly consistent with the step change in  $x$  at the 1994 periastron described in Section 5.6.

It is never-the-less striking that jumps at each periastron in projected semi-major axis *only* are required to satisfactorily model the data. Limits on changes to the other orbital parameters are at least an order of magnitude less than the values used in the simulations of Fig. 3. The systematic residual variations seen in Fig. 4b are well modeled by the step changes in  $x$  at each periastron and small adjustments in the other orbital parameters. If these variations are due to timing noise, the noise must mimic the effect of changes in the orbital parameters, that is, be smooth between periastrons and rapid near periastrons, which seems unlikely.

If the jumps in  $x$  are interpreted as changes in semi-major axis  $a$ , Kepler’s Third Law implies changes in  $P_b$  of order thousands of seconds, orders of magnitude larger than permitted by the timing solutions (cf. Fig. 3). The observed changes in  $x$  must then be interpreted as changes in inclination angle  $i$  of the orbit of order a few arcsec.

The question then is: what can cause changes in inclination angle without making significant perturbations to the other orbital parameters? Furthermore, the mechanism must be able to produce changes of different sign and magnitude at different periastrons.

There is evidence that the Be-star disk is highly inclined to the orbital plane both from observations of the pulsed emission (Johnston et al. 2001) and the unpulsed emission (Johnston et al. 1999), so the velocity of the disk material would have a significant component perpendicular to the orbit. In principle, frictional drag could then tilt the orbit. It is also known that the properties of the wind interaction vary substantially from orbit to orbit. The problem is that this effect could only change the orbit inclination with one sign and Manchester et al. (1995) suggest that the fractional change of orbital energy due to this effect is  $10^{-14}$ , too small to account for the observed changes.

The other possible mechanism appears to be tidal interactions occurring at each periastron (Papaloizou & Pringle 1982). As mentioned in Section 1, these effects can be greatly enhanced by resonances with modes of stellar oscillations. Since there is evidently a large angle between the spin axis and the orbit normal, again it is possible that the dominant effect could be on the orbit inclination. Different relative phases of the tides and stellar oscillations could alter the effect on the orbit from one periastron to the next. Calculations to date (e.g. Witte & Savonije 1999) have only considered aligned systems. However, once again, the predictions are that the effects would not be significant for PSR B1259–63 because of the relatively large ratio of periastron distance to companion-star radius.

## 7 CONCLUSIONS

We have presented an analysis of 13 years of timing data encompassing four periastron passages of PSR B1259–63. Significant changes in dispersion measure occurring near each periastron were accounted for in the data analysis. It is clear that secular changes in orbit parameters due to spin-orbit coupling does not give a good description of the data. The effect of timing noise is difficult to quantify because of coupling with the orbital parameters, a problem exacerbated by the long-duration eclipses which occur at each periastron. Consequently, we cannot rule out the possibility that our measured parameters are affected by timing noise. However, excepting the glitch which occurred near MJD 50691, the fact that within each orbit the observed residuals show variations with characteristic timescale of the same order as the orbital period and significant shorter-term variations only near the periastrons strongly suggests that changes in orbital parameters at periastron are the dominant effect. This is reinforced by the excellent fit to the data by a model containing the MJD 50691 glitch and steps in projected semi-major axis at each periastron. It is clear that these steps must result from step changes in the orbit inclination. However, we are unable to offer any plausible mechanism to account for the observed changes.

## ACKNOWLEDGMENTS

The Australia Telescope is funded by the Commonwealth of Australia for operation as a National Facility managed by the CSIRO. We would like to thank all the many pulsar observers who have contributed to collecting timing data

over the 13 years of this project. NW thanks NSFCC for support under project 10173020.

## REFERENCES

- Arzoumanian Z., Nice D. J., Taylor J. H., Thorsett S. E., 1994, *ApJ*, 422, 671
- Blandford R., Teukolsky S. A., 1976, *ApJ*, 205, 580
- Connors T. W., Johnston S., Manchester R. N., McConnell D., 2002, *MNRAS*, 336, 1201
- Cordes J. M., Downs G. S., 1985, *ApJS*, 59, 343
- Damour T., Deruelle N., 1986, *Ann. Inst. H. Poincaré (Physique Théorique)*, 44, 263
- Hirayama M., Cominsky L. R., Kaspi V. M., Nagase F., Tavani M., Kawai N., Grove J. E., 1999, *ApJ*, 521, 718
- Johnston S., Galloway D., 1999, *MNRAS*, 306, L50
- Johnston S., Lyne A. G., Manchester R. N., Kniffen D. A., D'Amico N., Lim J., Ashworth M., 1992a, *MNRAS*, 255, 401
- Johnston S., Manchester R. N., Lyne A. G., Bailes M., Kaspi V. M., Qiao G., D'Amico N., 1992b, *ApJ*, 387, L37
- Johnston S., Manchester R. N., Lyne A. G., Nicastro L., Spyromilio J., 1994, *MNRAS*, 268, 430
- Johnston S., Manchester R. N., Lyne A. G., D'Amico N., Bailes M., Gaensler B. M., Nicastro L., 1996, *MNRAS*, 279, 1026
- Johnston S., Manchester R. N., McConnell D., Campbell-Wilson D., 1999, *MNRAS*, 302, 277
- Johnston S., Wex N., Nicastro L., Manchester R. N., Lyne A. G., 2001, *MNRAS*, 326, 643
- Kaspi V. M., Tavani M., Nagase F., Hirayama M., Hoshino M., Aoki T., Kawai N., Arons J., 1995, *ApJ*, 453, 424
- Kaspi V. M., Bailes M., Manchester R. N., Stappers B. W., Bell J. F., 1996, *Nat*, 381, 584
- Lai D., 1997, *ApJ*, 490, 847
- Lai D., Bildsten L., Kaspi V. M., 1995, *ApJ*, 452, 819
- Lyne A. G., Manchester R. N., 1988, *MNRAS*, 234, 477
- Manchester R. N., Johnston S., 1995, *ApJ*, 441, L65
- Manchester R. N., 1996, in Johnston S., Walker M. A., Bailes M., eds, *Pulsars: Problems and Progress*, IAU Colloquium 160. Astronomical Society of the Pacific, San Francisco, p. 193
- Manchester R. N., Johnston S., Lyne A. G., D'Amico N., Bailes M., Nicastro N., 1995, *ApJ*, 445, L137
- Navarro J., 1994, PhD thesis, California Institute of Technology
- Papaloizou J. C. B., Pringle J. E., 1982, *MNRAS*, 200, 49
- Porter J. M., 2001, *MNRAS*, 280, 31
- Rankin J. M., 1983, *ApJ*, 274, 333
- Staveley-Smith L. et al., 1996, *Proc. Astr. Soc. Aust.*, 13, 243
- Tavani M., Arons J., 1997, *ApJ*, 477, 439
- Thomas B. M., Greene K. J., James G. L., 1990, *I.E.E.E. Trans. Ant. Propag.*, 38, 1898
- Wex N., 1998, *MNRAS*, 298, 997
- Wex N., Johnston S., Manchester R. N., Lyne A. G., Stappers B. W., Bailes M., 1998, *MNRAS*, 298, 997
- Witte M. G., Savonije G. J., 1999, *AA*, 350, 129